OXFORD
SOT | Society of Toxicology
academic.oup.com/toxsci

Toxicological Sciences, 2026, **209(5),** kfag048
https://doi.org/10.1093/toxsci/kfag048
Advance Access Publication Date: April 21, 2026
Research article

An environmentally relevant mixture of organophosphate esters induces cholesterol biosynthesis in THP-1 macrophages

Braeden H. Giles [1,2], Bernard Robaire [1,3], Koren K. Mann [1,2,*]

[1]Department of Pharmacology & Therapeutics, McGill University, Montreal, Canada
[2]Lady Davis Institute for Medical Research, McGill University, Montreal, QC, H3T 1E2, Canada
[3]Department of Obstetrics and Gynecology, McGill University, Montreal, QC, H3G 1Y6, Canada

*Corresponding author: Lady Davis Institute for Medical Research, McGill University, 3755 Cote Ste Catherine Road, Rm F202, Montreal, QC H3T 1E2, Canada. Email: koren.mann@mcgill.ca

Abstract

Organophosphate esters (OPEs), widely used as flame retardants and plasticizers, are environmental toxicants known to disrupt lipid metabolism. Although most studies have focused on individual OPEs, environmental exposures typically involve complex mixtures. Our previous studies demonstrated that a representative OPE mixture from Canadian household dust promotes cholesterol and lipid droplet accumulation in THP-1 macrophages. However, the molecular mechanisms underlying this lipid dysregulation remain unclear. Here, we employed tandem mass tag (TMT)-based quantitative proteomics to investigate how OPE mixtures alter protein expression and lipid regulation in macrophages. THP-1 macrophages were exposed to vehicle or environmentally relevant dilutions of the OPE mixture for 48 h. Lysates were subjected to TMT labeling and mass spectrometry. Bioinformatic analyses using STRING and Ingenuity Pathway Analysis identified 162 differentially expressed proteins, with unsupervised clustering highlighting cholesterol biosynthesis as a key pathway. Further validation via qPCR and upstream analysis implicated the sterol regulatory element-binding protein 2 (SREBP2) signaling axis in OPE-induced cholesterol biosynthesis. Functional assays revealed that atorvastatin-mediated HMG-CoA reductase inhibition, the rate limiting enzyme in cholesterol biosynthesis, prevents cholesterol buildup and lipid droplet formation in macrophages. These findings provide the first evidence that an environmentally relevant OPE mixture can induce cholesterol biosynthesis in human macrophages.
These studies provide mechanistic evidence that an environmentally relevant mixture of organophosphate esters induces cholesterol biosynthesis in macrophages. These findings link real-world exposure to lipid pathways implicated in metabolic disease and support the need for updated regulatory standards that protect human health.

Keywords: organophosphate esters; mixture; macrophage; lipid droplets; cholesterol biosynthesis; proteomics.

Graphical abstract

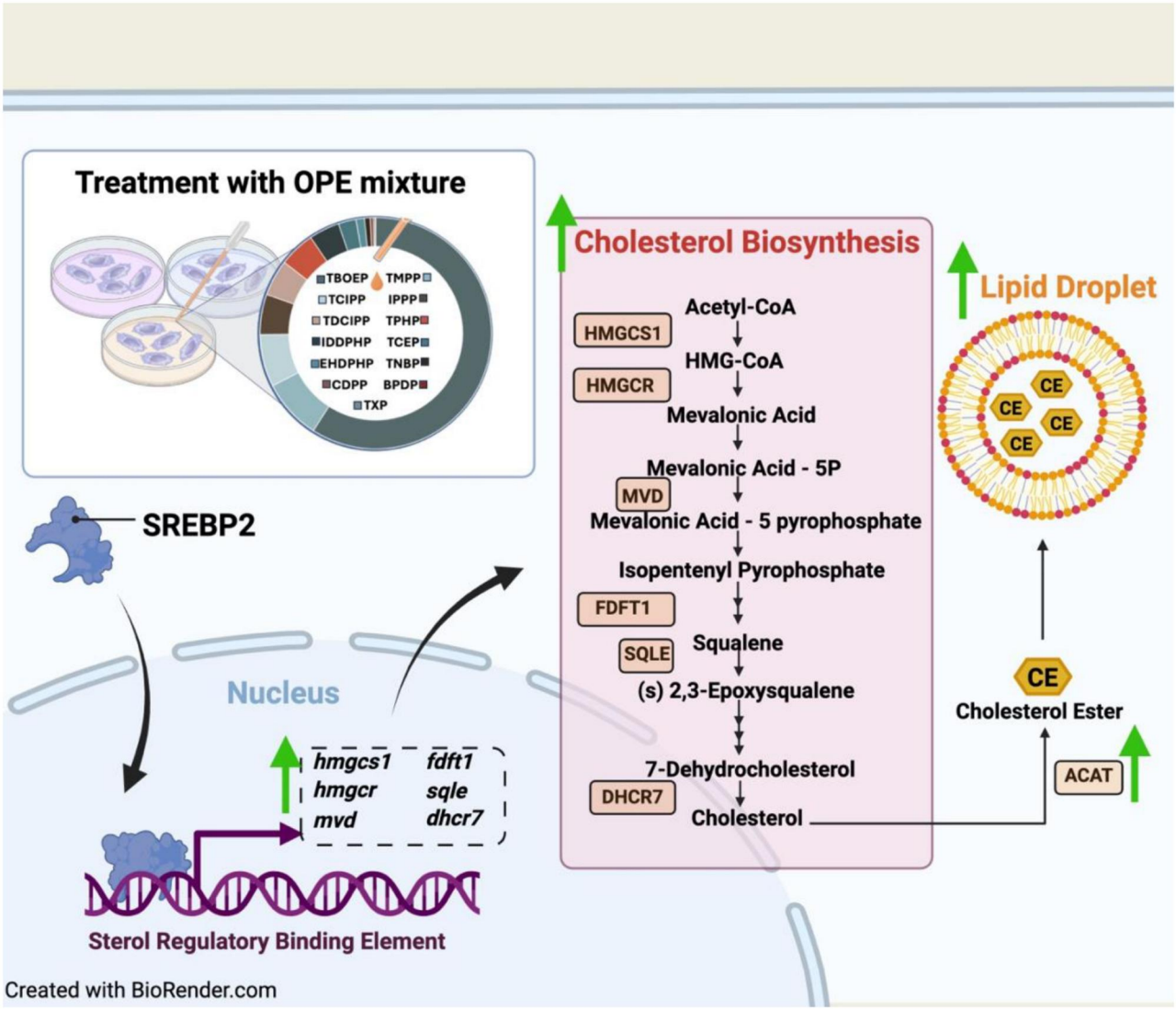

Organophosphate esters (OPEs) are semi-volatile compounds used as flame retardants, plasticizers, and hydraulic fluids in a range of consumer products (van der Veen and de Boer 2012; Blum et al. 2019; Dou and Wang 2023). With over 40 known chemical species, OPEs are highly versatile and are used in many applications (Huang et al. 2022; Wu et al. 2025). Most OPEs can be divided into one of three families—alkyl, aryl, or halogenated (van der Veen and de Boer 2012; Dou and Wang 2023). OPEs found widespread use following bans on brominated flame retardants, that have been largely phased out of production (van der Veen and de Boer 2012). Although initially introduced as an environmentally safer alternative compared with legacy chemicals (Zhang et al. 2016), emerging data challenge this assumption. OPEs are added to products and not covalently bound; thus, increasing their risk of environmental transport and accumulation (Rodgers et al. 2018; Blum et al. 2019). Indoor environments contribute to the majority of human exposure to OPEs via indoor house dust (Bastiaensen et al. 2019; Dou and Wang 2023). OPE-laden dust is transferred to hands or food, resulting in dermal and dietary exposure (Dou and Wang 2023). This is especially true in young children, who have disproportionate exposure to OPEs compared with adults as a result of increased hand-to-mouth behaviors (Doherty et al. 2019). The estimated daily intake for OPEs via ingestion is highest in Japan at 126.93 ng/kg bw/d for adults and 551.47 ng/kg bw/d for children (Dou and Wang 2023). In comparison, the estimated daily intake for Canadian adults and children is 14.74 ng/kg bw/d and 73.70 ng/kg bw/d, respectively (Dou and Wang 2023). Notably, the composition and levels of OPEs in dust are geospatially variable; this is largely attributed to differences in product use and regulation (Dou and Wang 2023).

Biomonitoring studies in humans and animal models have detected OPEs in hair, nails, urine, breast milk, placenta, amniotic fluid, and, concerningly, cord blood, an indicator of transplacental fetal exposure (Ding et al. 2016; Wang et al. 2021; Guo et al. 2022a). Numerous studies identify OPEs as toxicants in the immune, reproductive, adrenal, hepatic, and nervous system (Wade et al. 2019; Patisaul et al. 2021; Wang et al. 2022a; Yu et al. 2024; Giles et al. 2025). Although there are many system-specific effects, a common OPE-induced phenotype is lipid accumulation.

Across multiple *in vitro* models, OPEs increase the size and number of intracellular lipid droplets, indicating impaired lipid homeostasis (Hao et al. 2019; Wang et al. 2022a; Li et al. 2023a; Chen et al. 2024; Yu et al. 2024). Studies exploring these observations point to enhanced levels of triglycerides and/or cholesterol. In HepG2 liver cells, aryl OPEs increase both lipids, whereas halogenated OPEs preferentially increase triglycerides, with only tris (1,3-dichloro-2-isopropyl) phosphate (TDCIPP) raising cholesterol (Hao et al. 2019). This matches data in human trophoblasts and murine macrophages (Hu et al. 2019; Chen et al. 2024) exposed to the aryl OPE triphenyl phosphate (TPHP). However, effects are not strictly class-dependent; for instance, the aryl OPE 2-ethylhexyl diphenyl phosphate raises triglycerides without affecting cholesterol in H295R cells (Negi et al. 2025).

A limitation of most of these findings is their reliance on single chemical assessments. The ubiquitous application of OPEs in indoor environments results in human co-exposure. This is evidenced by studies in Australia, Canada, China, Europe, and the United States, where more than one OPE was detected in every analyzed sample (Fan et al. 2014; Cequier et al. 2015; Hoffman et al. 2017; He et al. 2018; Sun et al. 2018; Kubwabo et al. 2021; Ashley-Martin et al. 2023). Thus, studies using single OPEs lack a critical element of environmental relevance and are difficult to interpret from a risk perspective.

In a previous study (Giles et al. 2024), we addressed this limitation by utilizing an environmentally relevant mixture of OPEs that models Canadian exposure. We found that this mixture caused THP-1 macrophages to build up cholesterol and increase the number of intracellular lipid droplets. However, the mechanism(s) underlying the dysregulated lipid phenotype remain(s) unclear. The goal of the present study is to determine the mechanism(s) that drive OPE-induced cholesterol and lipid droplet accumulation in THP-1 macrophages. We hypothesize that by leveraging tandem mass tag (TMT) proteomics, we will be able to identify this mechanism and guide strategies to ameliorate the OPE-induced lipid phenotype.

Materials and methods

Chemicals and reagents

Details regarding the composition of the Canadian OPE house dust mixture, including chemical names, abbreviations, CAS numbers, Log(Kow), solubility, molecular weights, suppliers, and proportional representation have been described previously (Giles et al. 2024). A copy of this table has been included for reference (Table S1). This formulation consists of 13 OPEs that were detected in more than 85% of household dust samples collected from Canadian residences between 2007 and 2010 (Fan et al. 2014; Kubwabo et al. 2021). The mixture was prepared by Dr. Michael Wade at Health Canada. The undiluted OPE mixture was concentrated in dimethyl sulfoxide to a density of 1.124 mg/μl total OPEs; this is the equivalent of OPEs found in 6.32 g of house dust. At the highest exposure level utilized (a 1:20,000 dilution), the individual OPE concentrations (μg/g house dust) in 1 ml of solution reflect the median levels of exposure found in recent Canadian dust samples (Fan et al. 2014; Kubwabo et al. 2021). To aid in comparing our mixtures to available environmental data, the relative concentrations for the 1:100,000 and 1:20,000 dilutions as they would be found in solution has been included in Table 1.

Table 1. Relative concentrations of the 1:100,000 and 1:20,000 OPE dilutions in solution.

Chemical	1:100,000 (μM)	1:20,000 (μM)
Tris(2-butoxyethyl) phosphate (TBOEP)	16.66	83.31
Tris(methylphenyl) phosphate (TMPP)	2.58	12.88
Tris(1-chloro-2-isopropyl) phosphate (TCIPP)	2.51	12.54
Isopropylated triphenyl phosphate (IPPP)	1.40	6.98
Tris(1,3-dichloro-2-isopropyl) phosphate (TDCIPP)	1.32	6.60
Triphenyl phosphate (TPHP)	1.73	8.63
Isodecyl diphenyl phosphate (IDDPHP)	1.23	6.15
Tris(2-chloroethyl) phosphate (TCEP)	0.98	4.88
Ethylhexyl diphenyl phosphate (EHDPHP)	0.77	3.85
Tri-n-butyl phosphate (TNBP)	0.33	1.67
Cresyl diphenyl phosphate (CDPP)	0.16	0.79
Tert-butylphenyl diphenyl phosphate (BPDP)	0.06	0.28
Trixylyl phosphate (TXP)	0.03	0.15

Dulbecco's Modified Eagle Medium (DMEM, No. 319-005-CL), fetal bovine serum (FBS, No. 090150), phosphate-buffered saline (PBS, No. 311-425), 10X trypsin/EDTA (0.5% trypsin with 5.3 mM EDTA, No. 325-242), and 100× penicillin-streptomycin (No. 450-201) are from Wisent Bioproducts (Montreal, QC). Dimethyl sulfoxide (DMSO, No. D2650), phorbol 12-myristate 13-acetate (PMA; No. P8139), 2-mercaptoethanol (No. M3148), sodium hydroxide solution (No. 72068), and urea (No. U1250) are from SigmaAldrich (St Louis, MO). Bovine serum albumin (BSA, No. ALB001.100), Isopropyl alcohol (No. ISO920.1), sodium dodecyl Sulfate (SDS, No. SDS999.500), N-2-hydroxyethylpiperazine-N′-2-ethanesulfonic acid (HEPES, No. HEP005.100), and sterile water (No. WAT333.1) are from BioShop Canada Inc. (Burlington, ON). Atorvastatin (No. 10493) was purchased from Caymen Chemical (Ann Arbor, MI).

Cell culture and exposure to the OPE mixture

THP-1 cells (No. TIB-202) were obtained from the American Type Culture Collection (ATCC). Cultures were maintained at 37°C in a humidified atmosphere with 5% CO_2, using RPMI-1640 medium lacking phenol red. This medium was supplemented with 10% FBS, 0.5% penicillin-streptomycin, and 5×10^{-5} M 2-mercaptoethanol. All experiments utilized cells within 10 passages (~1 mo) following recovery from cryopreservation. Cells were cultured at densities ranging from 2.5 to 10×10^5 cells/ml, with media refreshed every 2 to 3 d.

THP-1-derived macrophages are a widely accepted model for human macrophage function, as differentiated cells exhibit key phenotypic markers and functional traits comparable to those of primary macrophages (Chanput et al. 2014). Monocytes were stimulated with 75 ng/ml PMA for 120 h to induce macrophage differentiation, with a medium change occurring after 72 h. This approach reflects a modified version of an established differentiation protocol (Daigneault et al. 2010).

Unless otherwise specified, THP-1 macrophages were differentiated as described above in 100 mm plates (VWR, Radnor, PA, No. 25384-088) and exposed to the OPE mixture for an additional 48 h prior to sample collection. The stock solution of the OPE mixture was diluted in culture media to create treatment groups. Two mixture dilutions are reported in this study (1:100,000; 1:20,000), and 0.5% DMSO was used as a vehicle control. Sets of samples were seeded and treated on independent days.

Tandem mass tag proteomics—generation of protein lysate

THP-1 macrophages (6×10^6 per plate) were washed three times with cold PBS to remove bovine proteins found in the FBS. Control and OPE (1:100,000; 1:20,000) treated macrophages were

lysed in 400 μl of a filter-sterilized alkaline-urea lysis buffer (8M urea, 0.15% SDS, 25 mM HEPES, sterile water, pH = 8) and transferred to a 2 ml Eppendorf tube on ice. Each sample was treated with 25 U/ml benzonase nuclease (SigmaAldrich, No. 70664) for 30 min on ice to degrade nucleic acids within the lysate and free bound nucleoproteins. Samples were then sonicated for 5 min on ice in 10-s pulses to aid in membrane degradation and protein solubilization. Lysates were then centrifuged at 13,000×*g* for 15 min at 4°C, and the supernatant was transferred to a new tube and frozen at −80°C until all samples were ready for downstream processing.

Tandem mass tag proteomics—peptide labeling and acquisition

TMT based quantitative proteomics enables accurate relative quantification by labeling peptides from different samples with isobaric tags of equal mass. These tags fragment during MS/MS to release reporter ions of distinct masses, allowing multiplexed analysis in a single run with reduced technical variability and improved precision over traditional semi-quantitative methods. To label the peptides, 100 μg of each sample was treated with TMT-16 plex reagents (ThermoFisher Scientific, Waltham, MA, No. A44521) according to the manufacturer's instructions. Labeled peptides were fractionated using Pierce High pH Reversed-Phase Peptide Fractionation Kit (ThermoFisher Scientific, No. 84868) into 8 fractions. Each fraction was re-solubilized in 0.1% aqueous formic acid and 2 μg of each was loaded onto a Thermo Acclaim Pepmap (Thermo, 75 μM ID×2 cm C18 3 μM beads) precolumn and then onto an Acclaim Pepmap Easyspray (Thermo, 75 μM×15 cm with 2 μM C18 beads) analytical column separation using a Dionex Ultimate 3000 uHPLC at 250 nl/min with a gradient of 2% to 35% organic (0.1% formic acid in acetonitrile) over 3 h running the default settings for MS3-level SPS TMT quantitation (McAlister et al. 2014) on an Orbitrap Fusion instrument (ThermoFisher Scientific) operated in DDA-MS3 mode.

Briefly, MS1 scans were collected at 120,000 resolution, scanning from 375 to 1,500 m/z, collecting ions for 50 ms or until the AGC target of 4e5 was reached. Precursors with a charge state of 2 to 5 were included for MS2 analysis, which were isolated with an isolation window of 0.7 m/z. Ions were collected for up to 50 ms or until an AGC target value of 1e4 was reached and fragmented using CID at 35% energy; these were then read out on the linear ion trap in rapid mode. Subsequently, the top 10 (height) sequential precursor notches were selected from MS2 spectra for MS3 quantitative TMT reporter ion analysis, isolated with an m/z window of 2 m/z, and fragmented with HCD at 65% energy. Resulting fragments were read out in the Orbitrap at 60,000 resolution, with a maximum injection time of 105 ms or until the AGC target value of 1e5 was reached.

Tandem mass tag proteomics—data analysis

To translate .raw files into protein identifications and TMT reporter ion intensities, Proteome Discoverer 2.2 (ThermoFisher Scientific) was used with the built-in TMT Reporter ion quantification workflows. Default settings were applied, with trypsin as the enzyme specificity. Spectra were matched against the human protein FASTA database obtained from Uniprot. Dynamic modifications were set as Oxidation (M) and Acetylation on protein N-termini. Cysteine carbamidomethyl was set as a static modification, together with the TMT tag on both peptide N-termini and K residues. All results were filtered to a 1% FDR (false discovery rate).

An intermediate dose (1:50,000) and fourth set of replicates was included in the original proteomic study design. During this stage of analysis, the 1:50,000 group and one set of replicates was removed as they did not pass quality control assessment on Proteome Discoverer 2.2. The .raw files for these data have been included in the data repository submission.

Statistical analysis was done using the abundance data from each sample. To identify proteins with altered expression, fold changes in expression levels ($\log_2$ scale) were calculated in comparison to control samples. Proteins were classified as differentially expressed if they exhibited a $\log_2$ fold change greater than 0.3 (up-regulated) or less than −0.3 (down-regulated) and an adjusted $-\log_{10}$ *P*-value of ≥1.3. Bioinformatics platforms such as STRING and Ingenuity Pathway Analysis (IPA) were used to explore protein clustering, interaction networks, and upstream molecular pathways. These analyses drew upon resources from databases including the Kyoto Encyclopedia of Genes and Genomes (KEGG), SWISS-PROT, and QIAGEN ingenuity dataset.

Quantitative polymerase chain reaction

Total RNA was extracted from 2×10^6 control or OPE (1:20,000) exposed THP-1 macrophages using TRIzol LS (Thermofisher Scientific, No. 10296010) following the manufacturer's protocol. A NanoDrop 2000 spectrophotometer (ThermoFisher, Waltham, MA, United States) was used to assess the concentration and purity of the extracted RNA. Primers were designed using the National Institute of Health primer-BLAST predictive design tool with requirements for exon-exon spanning to increase target specificity. Forward and reverse primer sequences were purchased as lyophilized DNA oligonucleotides from Integrated DNA Technologies (IDT, Coralville, IA).

Total RNA (500 ng) was converted to cDNA using the iScript cDNA synthesis kit (Bio-Rad Laboratories, Hercules, CA, No. 1708891). The converted cDNA (5 ng/well) was then combined with 400 nM of the primers listed in Table S2 and 1x GoTaq qPCR Master Mix (Promega, Maddison, WI, No. A6001). Quantitative PCR was done using an AB7500 Fast Thermocycler (Thermofisher Scientific). Each reaction was done in triplicate and averaged. Expression levels were normalized to eukaryotic18S ribosomal rRNA (*18 s*), which was detected using a FAM/MGB probe (Thermofisher Scientific, No. 4333760T). The results were analyzed using the ΔΔCt method.

Evaluation of cellular cholesterol

Total cholesterol in THP-1 macrophages was measured using an AMPLEX red cholesterol assay kit (Thermofisher Scientific, No. A12216). After complete differentiation, THP-1 macrophages were exposed to 0.5% DMSO, atorvastatin, the OPE mixture (1:20,000), or a combination of the OPE mixture and atorvastatin. Atorvastatin was used at 25 μM, a dose that inhibits >60% of HMG-CoA reductase activity and is below the cytotoxic limit (40 μM) for THP-1 macrophages (Qiu and Hill 2007).

After treatment, cells were collected, washed 3x in cold PBS, and then 5×10^5 cells were lysed using a 7:11:0.1 solution of chloroform (CX1005-2; EMD), isopropanol (A416-1; Fisher), and IGEPAL CA630 (No. 18896; Sigma-Aldrich) concomitant with sonication. The organic layer was isolated and concentrated in a SpeedVac Plus (Savant, Hyannis, MA, SC110A) by centrifuging in a 60°C vacuum chamber for 30 min at the default speed. The organic condensate was resuspended in 400 μl of reaction buffer and loaded into a 96-well plate. Total cholesterol was measured using a BioTek Synergy LX micromode reader (Agilent, Santa Clara, CA) at 530/590 excitation/emission following kit

instructions. Raw values were calculated using a cholesterol standard curve. Both the standard curve and sample measurements were done in duplicate.

Confocal microscopy

THP-1 macrophages (5×10^5 cells/well) were differentiated in a 12-well plate containing an ethanol-sterilized coverslip (Warner Instruments, Holliston, MA, No. 64-0733). After complete differentiation, THP-1 macrophages were treated with either 0.5% DMSO, 25 μM atorvastatin, the OPE mixture (1:20,000), or a combination of the OPE mixture and atorvastatin. Following treatment, the cells were fixed using 4% paraformaldehyde (PFA) before staining with a combination of 20 μM BODIPY 493/503 and 10 μg/ml Hoechst 33342 for 20 min at 37°C. Cells were then washed 3 times with PBS and mounted with prolong gold antifade liquid mountant (ThermoFisher Scientific, No. P36930). THP-1 macrophages were imaged on the Zeiss LSM800 (Zeiss, Oberkochen, Germany). Experiments were done with technical duplicates. CellProfiler (version 4.2.1) was used to quantify lipid droplet numbers.

Statistics

Data were analyzed using GraphPad Prism (version 10.1.0; GraphPad Software, Inc.). The number of independent experiments (experiments conducted on different days) is documented as "*n*=" for each assay in the corresponding figure legend. Where technical duplicates or triplicates are used, the average of the technical replicates is equal to one independent experiment. Data pertaining to qPCR, microscopy, and cholesterol were analyzed by one-way analysis of variance (ANOVA) followed by a Tukey's or Welch's *t*-test for multiple comparison testing. For all data presented, the minimal level of significance was $P \leq 0.05$. All datasets were tested for outliers using a Grubbs statistical outlier test. All outliers were removed prior to statistical analyses.

Results

Exposure to the OPE mixture alters macrophage protein expression

Previously, we reported that THP-1 cholesterol levels were significantly increased by an OPE mixture at a dilution of 1:20,000, but were unaffected at 1:100,000 (Giles et al. 2024). Increased cholesterol levels correlated with cytoplasmic lipid accumulation, although the mechanism(s) by which OPEs increased lipids remained unclear. Notably, 1:20,000 is also the highest non-cytotoxic concentration tolerated by THP-1 cells (Giles et al. 2024). As such, we compared macrophages exposed to these two doses to assess differentially expressed proteins (DEPs) that also correlated with lipid accumulation in order to elucidate potential mechanisms.

TMT-proteomic analysis of 1:100,000 and 1:20,000 dose groups identified 3,342 proteins consistently detected across all technical replicates. Abundance scores from all 3,342 proteins were used to visualize the degree of separation between the control, 1:100,000 and 1:20,000 groups (Fig. 1A). 1:20,000 exposure resulted in a complete proteomic separation from both the control and 1:100,000 groups by two-dimensional principal component analysis (2D-PCA). In contrast, the confidence interval of the 1:100,000 group overlaps with control samples, suggesting limited separation between the 1:100,000 and control samples.

An analysis of differential expression identified 162 proteins that were significantly altered relative to controls ($Log_2FC \pm 0.3$; $P < 0.05$). Tables of the top 10 up-regulated and down-regulated DEPs in the 1:100,000 and 1:20,000 dose groups are shown in Tables S3 and S4. As expected, the 1:20,000 group exhibited a greater number of DEPs compared with the 1:100,000 group (Fig. 1B). In both exposure groups, there were more down-regulated proteins than up-regulated proteins, suggesting that the OPE mixture is more suppressive than inductive concerning macrophage protein expression.

To further assess the nature of identified DEPs, we plotted significance versus fold change for each OPE dilution vs. control (Fig. 1C and D). This revealed that the higher number of DEPs in the 1:20,000 OPE dilution group is not the only distinguishing feature. In the 1:100,000 condition, most DEPs were concentrated near the log_2 fold change threshold (Fig. 1C), suggesting more modest alterations in protein abundance. In contrast, the 1:20,000 treatment yielded DEPs with both higher statistical significance and greater fold changes (Fig. 1D), indicating more substantial proteomic disruption. These data suggest that OPE-induced effects are not only more numerous but also more pronounced at higher exposure levels.

Of the 162 total DEPs, 139 occurred only in the 1:20,000 vs. control analysis and 14 occurred only in the 1:100,000 vs. control analysis. The remaining 9 DEPs occurred in both the 1:20,000 vs. control and 1:100,000 vs. control analysis (Table S5). All overlapping DEPs exhibited similar directional changes and were either up-regulated or down-regulated in both exposure groups (Table S5). The majority of overlapping proteins demonstrated dose-dependency, with a minority displaying comparable fold changes between low and high dose conditions.

Functional interaction network and pathway analysis

To identify biological functions that contribute to lipid accumulation, we conducted an enrichment analysis utilizing STRING followed by unsupervised clustering. Analysis of DEPs from the 1:100,000 group revealed functional interactions for 9 of the 23 listed proteins (Fig. S1A). These functions were predominantly nuclear and mitochondrial in nature, such as histone methylation, mRNA preprocessing, respiratory electron transport, and mitochondrial pore formation.

A STRING pathway enrichment was also conducted on the DEPs that were shared between the 1:20,000 vs. control and 1:100,000 vs. control analysis. DEPs from the overlapping protein set revealed functional interactions for 3 of the 9 listed proteins. The singular functional association identified in the overlapping protein set was disruption to respiratory electron transport (Fig. S1B).

Because the 1:100,000 treatment condition shared a considerable overlap on the 2D-PCA with control samples, we chose to combine DEPs from both conditions for mechanistic analysis. This approach enabled a more robust evaluation of functional networks. In the combined analysis, 92 of the 162 DEPs had functional interactions spread across 25 identified clusters (Fig. 2A; Table S6). Preluded in the overlapping DEP analysis, many DEPs in the combined analysis were associated with nuclear and mitochondrial functions. These include RNA transcription, mitochondrial membrane transport, and respiratory electron transport. Unlike the 1:100,000 vs. control analysis, the combined dataset also highlighted immune cell activation and lipid homeostasis as impacted functions, specifically, myeloid leukocyte activation, lipid metabolism, and cholesterol biosynthesis.

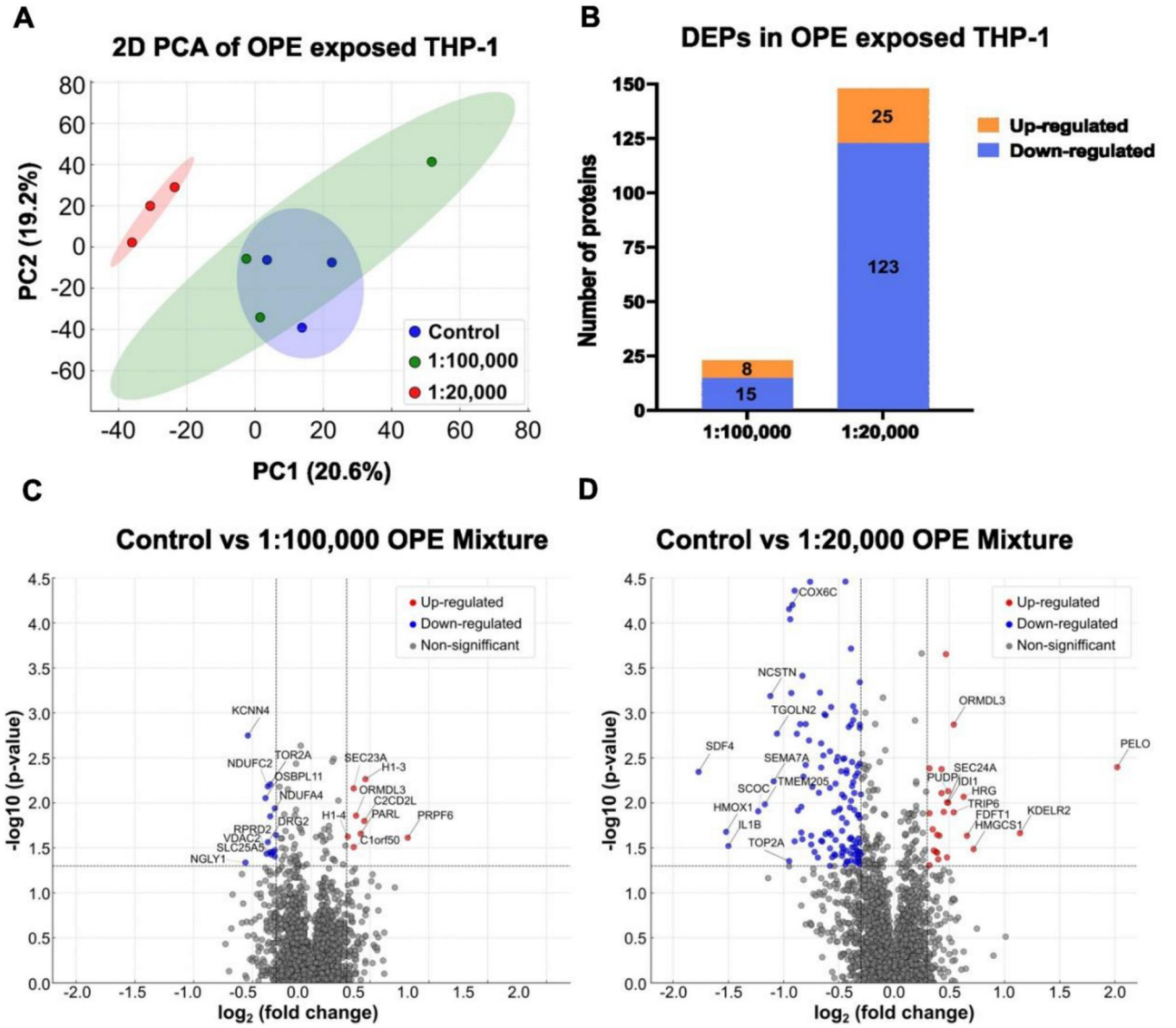

Fig. 1. Assessment of THP-1 macrophage proteomes following exposure to a mixture of OPEs. (A) Principal component analysis showing the degree of separation between control ($n = 3$; blue), 1:100,000 ($n = 3$; green), and 1:20,000 ($n = 3$; red) dilutions of the OPE mixture. Ellipses represent confidence intervals (95%) for each group. (B) Bar graphs representing the number of DEPs across exposure conditions and trends in up-regulated (orange) and down-regulated (blue) proteins. (C, D) Differentially expressed proteins (log2 fold change ≥ |0.3|, p = −log10 ≥ 1.3) between control and OPE-exposed THP-1 macrophages at (C) 1:100,000 and (D) 1:20,000 dilutions; visualized using a volcano plot. Top 10 up-regulated (red) and down-regulated (blue) proteins by log2 fold change values are shown.

Proteins involved in mitochondria, RNA transcription/translation, and immune activation

Hierarchical Z score clustering of proteins related to mitochondria, RNA transcription, and immune activation (Fig. S2) revealed consistent group-specific expression patterns. Exposure to the 1:20,000 OPE dilution decreased all proteins linked to mitochondria and all but four linked to RNA transcription and immune activation. In the 1:100,000 group (Fig. S2), most proteins exhibited small to moderate changes, whereas the 1:20,000 dilution induced the most pronounced alterations, suggesting dose dependence. There were four major superfamilies that were identified: Subunits of complexes I (NDUF proteins) and IV (COX proteins) in the electron transport chain (ETC), subunits of RNA polymerase II (POLR proteins), and cytokines/chemokines. Complex I and complex IV of the ETC produce the majority of the proton motive force required to generate ATP (Nolfi-Donegan et al. 2020). RNA polymerase II is a required protein for the synthesis of mRNA (Reines 2020). The chemokines/cytokines interleukin-1 beta (IL1β), IL18, transforming growth factor beta 1 (TGFβ1), CC chemokine 5 (CCL5), and macrophage colony-stimulating factor (CSF1) are involved in the process of recruitment, differentiation, and activation of macrophages (Shi and Pamer 2011; Arango Duque and Descoteaux 2014; Li et al. 2023b). These protein patterns would support the hypothesis that OPEs decrease monocyte recruitment, macrophage differentiation, mRNA transcription, and induce bioenergetic impairment.

Proteins involved in lipid metabolism and biosynthesis

Among the clusters identified in the STRING analysis (Fig. 2A), lipid/cholesterol metabolism and cholesterol biosynthesis relate directly to lipid regulation. Hierarchical clustering of Z score normalized proteins within these clusters revealed that samples from the 1:100,000 dilution did not form a distinct grouping (Fig. 2B).

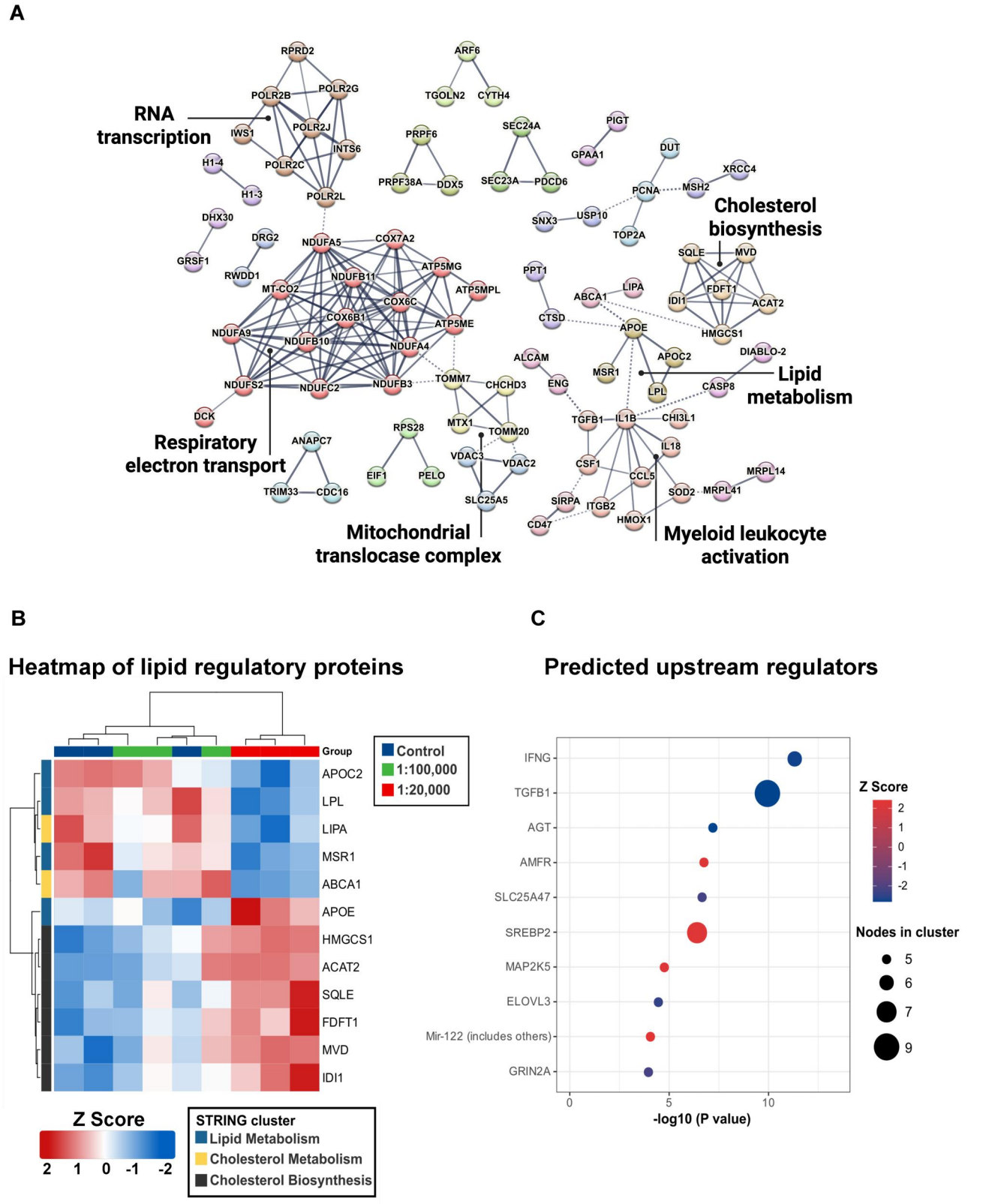

Fig. 2. STRING network clustering of differentially expressed proteins with heatmap of lipid metabolism and regulatory protein expression following OPE exposure. (A) Functional network analysis of 162 proteins identified as DEPs following exposure to either the 1:100,000 ($n = 3$) or 1:20,000 ($n = 3$) of the OPE mixture. DEPs were analyzed using STRING (high-confidence interaction score = 0.7) and clustered via the Markov Cluster Algorithm (inflation parameter = 2). Major clusters (≥4 proteins) are annotated. A complete list of major and minor clusters can be found in Table S6. (B) Heatmap of Z score normalized abundance for proteins identified in STRING clusters for lipid metabolism, cholesterol metabolism, and cholesterol biosynthesis. Treatment groups: Control (blue), 1:100,000 dilution (green), and 1:20,000 dilution (red) of the OPE mixture. Z score normalization was by row. Wards method (Ward.D2) was used for clustering. (C) Bubble plot of the top ten upstream regulators identified through Ingenuity Pathway Analysis. *X*-axis: −log10 p-values organized from most to least significant. *Y*-axis: Corresponding upstream regulators. Bubble size: Number of connections between the upstream regulators and heatmap (B) proteins. Bubble color: Predicted change in regulator activity by OPE mixture (red = induced, blue = inhibited). Upstream analysis was performed on all 162 DEPs from the combined dataset and filtered to contain only the regulators with ≥5 heatmap proteins as connected nodes. Figures created on HiPlot.cn.

Instead, they intermixed with control replicates, indicating limited separation between these treatment groups. In contrast, samples exposed to 1:20,000 dilution of the OPE mixture had clear group-specific expression patterns (Fig. 2B). Quantitative analysis of raw protein abundance (Fig. S3) confirms that significant alterations were primarily confined to the 1:20,000 dilution group. In the 1:100,000 group, only the reduction in macrophage scavenger receptor 1 (MSR1) reached statistical significance (Fig. S3).

Unlike the mitochondrial, transcriptional, and inflammatory STRING clusters, proteins involved in lipid regulation did not show a consistent pattern of down-regulation. Instead, they displayed a balanced distribution of up- and down-regulated proteins, which were segregated by synthesis and metabolism. Proteins associated with lipid uptake and efflux, such as MSR1 and ATP-binding cassette transporter A1 (ABCA1), in addition to lipoprotein lipase (LPL) and lysosomal acid lipase A (LIPA) were decreased. These data suggest impaired processing of lipoproteins and lipid droplets into fatty acids (FAs) and cholesterol with compensatory reductions in uptake and efflux. In contrast, proteins involved in cholesterol biosynthesis were up-regulated, along with ACAT2, which esterifies free cholesterol for storage in lipid droplets. These findings suggest three mechanisms (impaired lipid catabolism, impaired lipid efflux, and enhanced cholesterol synthesis) that would promote lipid accumulation in macrophages.

To identify mechanistic regulators, an upstream analysis was done using IPA. The analysis was filtered to include the top ten upstream regulators with direct or indirect connections to proteins in the lipid regulatory clusters (Fig. 2C). The upstream regulators that were most connected were TGFβ1, interferon gamma (IFNγ), and sterol regulatory element-binding protein 2 (SREBP2). Although both TGFβ1 and IFNγ are associated with the inhibition of cholesterol biosynthesis, it is unclear if they act as direct regulators or through intermediaries (Lee et al. 2008; Wang et al. 2024a). In contrast, SREBP2 directly binds sterol regulatory binding elements (SREs) in the promoters of genes that catalyze cholesterol biosynthesis and is considered the master regulator (Mazein et al. 2013). Notably, SREBP2 is not known to control lipid uptake or lipase expression. This suggests that additional regulatory pathways may be involved that were not captured in the upstream analysis.

Effect of OPEs on SREBP2 transcription and downstream targets

SREBP2 is synthesized as an inactive precursor in the endoplasmic reticulum and requires proteolytic cleavage to release its active N-terminal fragment, which translocates to the nucleus (Mazein et al. 2013). There, it binds SREs to induce transcription of over 20 enzymes in the cholesterol biosynthesis pathway (Mazein et al. 2013). A simplified schematic highlighting this pathway and proteins identified utilizing STRING analysis is shown in Fig. 4A. As hierarchical clustering and quantified analysis (Fig. 2B and Fig. S3) identified only the 1:20,000 dilution of the OPE mixture as a significant driver of cholesterol biosynthesis, the 1:100,000 dilution as a treatment group was discontinued hereafter.

To investigate the impact of the OPE mixture on SREBP2 transcription and downstream targets, RNA was collected from an independent set of OPE-treated THP-1 macrophages not used in the proteomic analysis. We measured transcript levels of *srebf2*, which encodes SREBP2, and the well-known target genes 3-hydroxy-3-methylglutaryl-CoA reductase (HMGCR) and squalene epoxidase (SQLE). Exposure to the 1:20,000 dilution of the OPE mixture significantly increased *srebf2* transcript levels compared with control cells (Fig. 3B). This was accompanied by a significant up-regulation of transcripts for *hmgcr* and *sqle* (Fig. 3C and D). These data support the hypothesis that OPEs induce cholesterol biosynthesis through an SREBP2 mediated signal pathway.

Effect of atorvastatin blockade on OPE-induced lipid accumulation

Although elevated transcript levels of cholesterol biosynthetic enzymes suggest increased pathway activity, they are an indirect determination of increased cholesterol biosynthesis. We next directly assessed this pathway. To do this, we pharmacologically inhibited the pathway using atorvastatin, a competitive inhibitor of HMGCR, which inhibits the conversion of HMG-CoA into mevalonic acid (Fig. 4A). Exposure to the 1:20,000 dilution of the OPE mixture resulted in a significant increase in total cholesterol levels (Fig. 4B). Co-exposure of the OPE mixture with 25 μM of atorvastatin resulted in a significant reduction in total cholesterol when compared with the OPE treatment group alone (Fig. 4B). The OPE-atorvastatin co-exposure group was not significantly different from the vehicle control or atorvastatin only groups (Fig. 4B). This suggests that cholesterol biosynthesis is responsible for cholesterol accumulation in OPE-exposed THP-1 macrophages.

To determine whether the decrease in cholesterol observed during OPE and atorvastatin co-exposure also affected lipid droplet accumulation in THP-1 macrophages, we stained the cells with BODIPY 493/503. As expected, THP-1 macrophages exposed to the 1:20,000 dilution of the OPE mixture exhibited a significant increase in cytoplasmic lipid droplets compared with controls (Fig. 4C and D). When co-treated with 25 μM atorvastatin, we observed a significant reduction in lipid droplet accumulation relative to OPE-treated macrophages (Fig. 4C and D). These findings suggest that cholesterol biosynthesis is a key pathway in OPE-induced lipid droplet formation.

Discussion

Macrophages maintain lipid homeostasis through multiple pathways, including cholesterol biosynthesis, lipid import, and fatty acid synthesis, which when disrupted can lead to lipid accumulation. Quantitative proteomics and in silico clustering identified several differentially expressed protein networks in OPE-exposed macrophages, with cholesterol biosynthesis emerging as a consistent mechanism. This interpretation is further strengthened by qPCR analyses in an independent set of OPE-exposed macrophages, which showed increased mRNA transcripts of the cholesterol biosynthesis enzymes *hmgcr* and *sqle*. Notably, these findings are consistent with studies utilizing individual OPEs in nonimmune cell types (Hao et al. 2019; Yu et al. 2025).

These findings align closely with our previous data, where OPEs induced cholesterol accumulation in THP-1 macrophages (Giles et al. 2024). Importantly, cholesterol accumulation does not increase at 1:100,000, but is obviously increased at a dose of 1:20,000. This outcome was recapitulated in the current study as differential expression of cholesterol associated proteins was restricted to the higher dose. As such, there is a strong correlation between phenotypic presentation and molecular mechanism in our macrophage model.

To directly test this mechanism, we co-treated macrophages with atorvastatin, an inhibitor of HMGCR, which attenuated OPE-induced cholesterol accumulation and lipid droplet formation. This effect is unlikely to reflect coincidental pathway

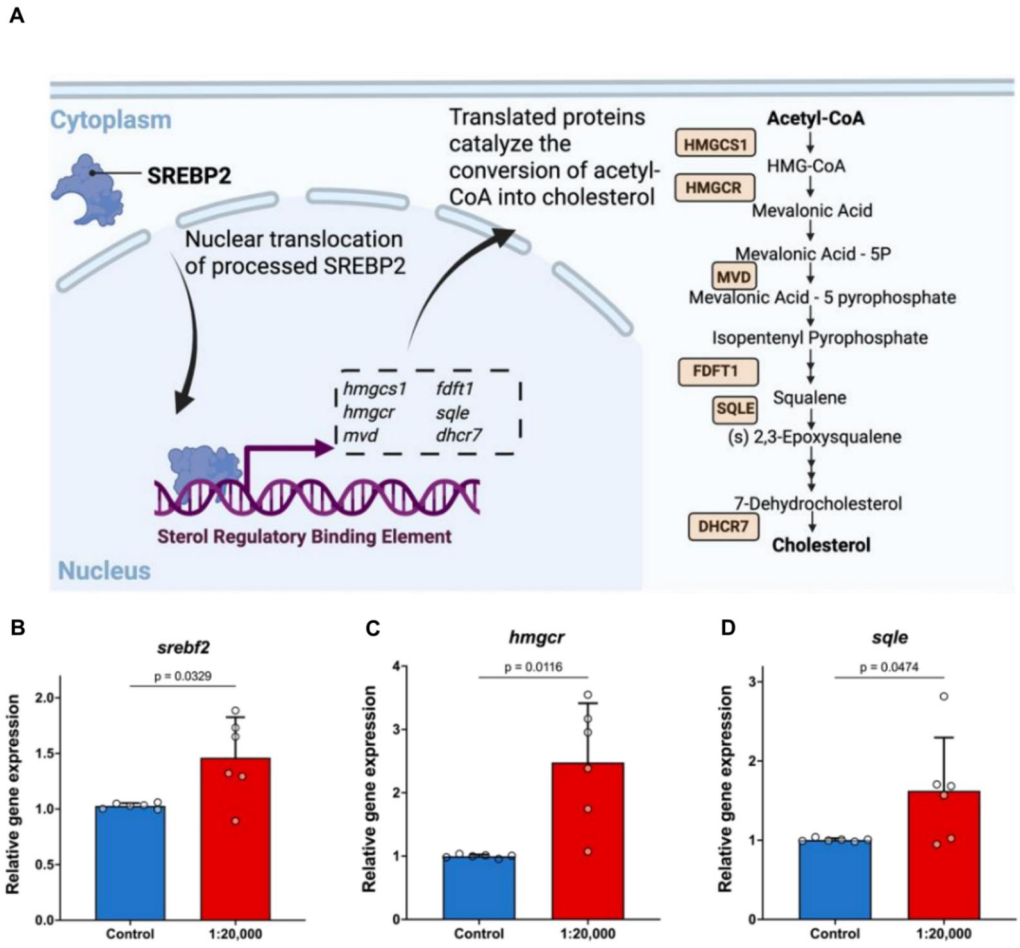

Fig. 3. SREBP2-mediated transcriptional regulation of cholesterol biosynthesis and quantification of select targets. (A) Schematic illustration of SREBP2 activation and downstream transcriptional control of cholesterol biosynthesis featuring proteins identified as differentially expressed in proteomic analysis. Translated proteins catalyze the stepwise conversion of acetyl-CoA into cholesterol. Illustration created on BioRender.com (B-D) Quantitative RT-PCR analysis of *srebf2*, *hmgcr*, and *sqle* transcript levels in THP-1 macrophages treated with a vehicle control or an OPE mixture (1:20,000 dilution). Data are presented as mean ± SD ($n = 6$). Samples were plated in technical triplicates, were averaged, and then normalized to an endogenous control (*18 s*). Fold change was calculated via double delta Ct method. Statistical analysis was performed using one-way ANOVA followed by Welch's *t*-test.

cancellation, as macrophages synthesize only ~0.1% of their cholesterol under basal conditions (Werb and Cohn 1971) and therefore lack sufficient endogenous synthesis to offset an independent mechanism. Collectively, these findings, and their connection to previous data, support OPE-induced *de novo* cholesterol synthesis as the primary mechanism underlying OPE-induced lipid accumulation.

Our data do not support the hypothesis that OPEs enhance the import of lipids from lipoprotein carriers. Lipid import in macrophages is mediated through lipoprotein phagocytosis or scavenger receptor-mediated pathways, including MSR1 (Remmerie and Scott 2018). Internalized lipoproteins are then degraded by lipases, such as LPL and its co-activator apolipoprotein C-II (APOC2), resulting in the release of FAs and cholesterol into the cytoplasm (Remmerie and Scott 2018). There are significant reductions in the import carrier MSR1, in addition to APOC2 and LPL. This indicates that OPE-treated macrophages are reducing their lipid intake and ability to extract lipids from lipoproteins, potentially as a compensatory mechanism to account for an overburdened state.

An additional pathway considered was fatty acid synthesis (FAS) as several individual OPEs upregulate FAS proteins (Hao et al. 2019; Wang et al. 2022b; An et al. 2023; Yang et al. 2025). An analysis of our combined proteomics dataset did not find the rate limiting FAS proteins ACC1 or FASN to be differentially expressed (Fig. S4). This indicates that FAS is unlikely to be a driver of lipid droplet accumulation following exposure to the OPE mixture.

Our Ingenuity Pathway Analysis identified several regulators that may represent upstream targets of the OPE mixture. Although we ultimately explored a hypothesis connected to the second most prominent regulator SREBP2, TGFβ1 signaling was considered due to the high number of predicated connections. TGFβ1 acts on lipid metabolism indirectly by activating suppressor of mothers against decapentaplegic (SMAD) signal pathways (Liu and Chen 2022; Wang et al. 2024a). Supplementation with TGFβ1 reduces *hmgcr*, *sqle*, and total cholesterol levels (Wang et al. 2024a). Given that TGFβ1 is decreased by OPE exposure (Fig. S2), it is plausible that TGFβ1 is involved in the modulation of cholesterol homeostasis by OPEs. However, TGFβ1 is also a regulator of FAS (Samuel et al. 2002; Yadav et al. 2011). Thus, the lack of protein expression alterations in FAS pathways does not align with down-regulation of TGFβ1 being the master regulator of OPE-induced lipid dysregulation (Fig. S4).

In addition to cholesterol biosynthesis and lipid metabolism, STRING analysis identified several other protein clusters that

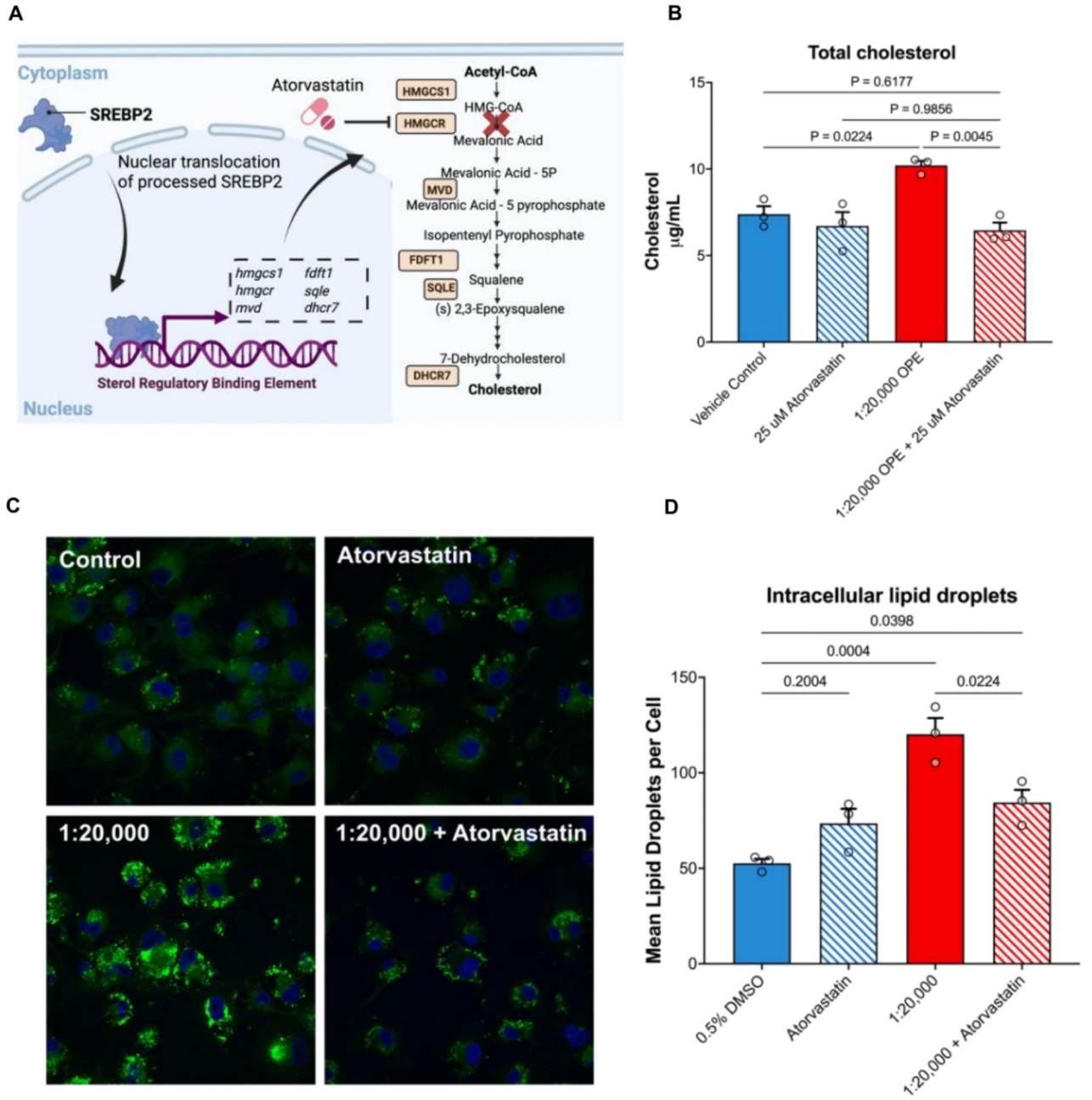

Fig. 4. Impact of Atorvastatin on OPE-induced lipid accumulation. (A) Schematic showing inhibition of the cholesterol biosynthesis pathway by atorvastatin, a competitive inhibitor of HMGCR. Illustration created on BioRender.com. (B) Quantification of total cholesterol levels in THP-1 macrophages following exposure to vehicle control, 1:20,000 dilution of the OPE mixture, 25 μM atorvastatin alone, or co-treated OPE and atorvastatin. (C) Representative confocal images of BODIPY-stained lipid droplets (green) and DAPI-stained nuclei (blue) across treatment groups. (D) Quantification of mean lipid droplets in THP-1 macrophages exposed to the same treatment paradigm as (B). Data are presented as mean ± SD ($n = 3$). For each n, samples were plated or stained in technical duplicates and averaged. Statistical analysis was performed using one-way ANOVA followed by Tukey's multiple comparison test.

were altered by OPE exposure. These include mitochondrial electron transport, RNA transcription, and macrophage activation. Interestingly, mitochondrial proteins corresponding to the NADH dehydrogenase [ubiquinone] and cytochrome c oxidase (COX) families, which encode subunits of electron transport chain Complexes I and IV (Nolfi-Donegan et al. 2020), were downregulated following OPE exposure. Cellular cholesterol accumulation shares a potential connection with mitochondrial dysfunction. Elevated mitochondrial cholesterol prevents cytoplasmic glutathione from translocating into the mitochondrial lumen, reducing antioxidant capacity (Goicoechea et al. 2023). Once depleted of antioxidants, oxidative stress damages mitochondrial proteins and accelerates protein turnover, which, if exceeding replacement, can present as reduced protein abundance (Pratt et al. 2002).

The anticipated outcome of downregulated ETC proteins is a decrease in mitochondrial membrane potential (MMP). Notably, this stands in contrast to our previous report that the OPE

mixture does not alter MMP in THP-1 macrophages (Giles et al. 2024). One possibility for this is that the tracking compound used for assessment of MMP may not have been sensitive enough to detect subtle or dynamic changes in the MMP of OPE-exposed THP-1. As such, further research into the impact of the OPE mixture on mitochondrial function is warranted.

OPE-induced cholesterol accumulation also carries important implications for macrophage activation via inflammatory signaling. Cholesterol accumulation in macrophages is typically associated with elevated levels of IL-18 and IL-1β (Tall and Yvan-Charvet 2015). We observe the anticipated upregulation of IL-18; however, we report a decrease in IL-1β (Fig. S2). This may reflect the distinct regulatory dynamics of these cytokines. IL-18 is constitutively expressed and rises with cholesterol accumulation via lysosomal destabilization and subsequent NLRP3 inflammasome assembly (Zhu and Kanneganti 2017). Our previous work found that the OPE mixture decreases the intensity of lysosomal markers (Giles et al. 2024). This would fit a pattern of cholesterol-mediated lysosomal disruption and offers a mechanistic basis for the enhanced IL-18 levels observed here. In contrast, IL-1β is transiently expressed and subject to more stringent regulation (Zhu and Kanneganti 2017). As such, the reduced IL-1β expression in our dataset may indicate that an initial inflammatory response has already subsided and is now being actively suppressed to maintain cellular homeostasis. Continued work in this area will be critical in understanding the impact OPEs have on immune signaling and inflammatory disease outcomes.

A notable limitation of this work is that our results may be specific to monocyte-derived macrophages. THP-1 macrophages originate from immortalized monocytes and therefore, model monocyte-derived macrophages (Daigneault et al. 2010). We used this cell line to reduce variability and clarify the underlying mechanism; however, many *in vivo* macrophage populations are not monocyte-derived. Instead, they arise from fetal-liver precursors (Guan et al. 2025). These long-lived "resident" macrophages have distinct lipid metabolism and synthesis utilized for diverse and distinct functions (Remmerie and Scott 2018). As a result, our work in THP-1 cells may not reflect OPE-induced responses across all macrophage types.

Although this study focused on mechanisms driving OPE-induced cholesterol and lipid droplet accumulation in THP-1 macrophages, the broader health implications are important to consider. Cholesterol biosynthesis is highly conserved across cell types suggesting these effects may extend beyond the immune system. Consistent with this, TNBP, TPHP, TCIPP, and TDCIPP upregulate transcriptional drivers of cholesterol biosynthesis in hepatic tissue (Hao et al. 2019; Wang et al. 2022b; An et al. 2023; Yang et al. 2025). These findings also align with our prior observations of lipid accumulation in hepatocytes and cholesterol accumulation in human granulosa and liver cells exposed to the same mixture (Wang et al. 2024b; Yu et al. 2025).

At the population level, enhanced cholesterol biosynthesis and disrupted metabolism raise concerns for outcomes such as cardiometabolic disease, in which cholesterol plays a critical role. These concerns are supported by epidemiological associations between OPE exposure and coronary heart disease, cardiovascular disease, metabolic syndrome, and obesity (Luo et al. 2020; Guo et al. 2022b; Zhang et al. 2024). Understanding these mechanisms is therefore critical for predicting health risks and informing our ultimate goal of updating regulatory standards to protect our population from widespread, unintentional exposure.

Acknowledgments

We thank Dr Michael G. Wade (Health Canada) for providing the OPE house dust mixture. We also thank Amy Wong, Jenna Cleyle, and Lorne Taylor from the McGill University Health Center Proteomics and Molecular Analysis Platform for their help in peptide processing, MS/MS acquisition, and data analysis.

Author contributions

Braeden H. Giles: Writing—review & editing, Writing—original draft, Visualization, Methodology, Investigation, Formal analysis, Data curation, Conceptualization. Bernard Robaire: Writing—review & editing, Visualization, Supervision, Resources, Project administration, Funding acquisition, Conceptualization. Koren K. Mann: Writing—review & editing, Visualization, Supervision, Resources, Project administration, Funding acquisition, Conceptualization.

Supplementary material

Supplementary material is available at *Toxicological Sciences* online.

Funding

This research was made possible thanks to the support of the Lady Davis Institute/Galina Dorfman Graduate Fellowship Award/Martin Brook Scholarship. Other sources of funding include the Canadian Institutes of Health Research (CIHR), Institute for Population and Public Health Team Grant (FRN IP3-150711), Canadian Institutes of Health Research (CIHR) Project Grant (FRN 156239), Heart and Stroke Foundation of Canada (G-23-0034943), and McGill University. B.H.G. is the recipient of training awards from the Centre for Research in Reproduction and Development (CRRD). B.R. is a James McGill Professor.

Conflicts of interest. None declared.

Data availability

The mass spectrometry proteomics data have been deposited to the ProteomeXchange Consortium via the PRoteomics IDEntifications database (PRIDE) partner repository with the dataset identifier PXD067007. Data for all other experiments are available upon request.

Declaration of generative AI and AI-assisted technologies in the writing process

During the preparation of this work, B.H.G. used ChatGPT-4o with information sharing disabled in order to correct grammar and improve the readability and language of the manuscript. After using this tool/service, B.H.G., B.R., and K.K.M. reviewed and edited the content as needed and take full responsibility for the content of the published article.

Disclosure summary

None of the authors has anything to disclose.

References

An J, Jiang J, Tang W, Zhong Y, Ren G, Shang Y, Yu Z. 2023. Lipid metabolic disturbance induced by triphenyl phosphate and hydroxy metabolite in HEPG2 cells. Ecotoxicol Environ Saf. 262:115160. https://doi.org/10.1016/j.ecoenv.2023.115160

Arango Duque G, Descoteaux A. 2014. Macrophage cytokines: involvement in immunity and infectious diseases. Front Immunol. 5:491. https://doi.org/10.3389/fimmu.2014.00491

Ashley-Martin J, MacPherson S, Zhao Z, Gaudreau E, Provencher G, Fisher M, Borghese MM, Bouchard MF, Booij L, Arbuckle TE. 2023. Descriptive analysis of organophosphate ester metabolites in a Pan-Canadian Pregnancy cohort. Sci Total Environ. 883:163327. https://doi.org/10.1016/j.scitotenv.2023.163327

Bastiaensen M, Ait Bamai Y, Araki A, Van den Eede N, Kawai T, Tsuboi T, Kishi R, Covaci A. 2019. Biomonitoring of organophosphate flame retardants and plasticizers in children: associations with house dust and housing characteristics in Japan. Environ Res. 172:543–551. https://doi.org/10.1016/j.envres.2019.02.045

Blum A, Behl M, Birnbaum L, Diamond ML, Phillips A, Singla V, Sipes NS, Stapleton HM, Venier M. 2019. Organophosphate ester flame retardants: are they a regrettable substitution for polybrominated diphenyl ethers? Environ Sci Technol Lett. 6:638–649. https://doi.org/10.1021/acs.estlett.9b00582

Cequier E, Sakhi AK, Marce RM, Becher G, Thomsen C. 2015. Human exposure pathways to organophosphate triesters—a biomonitoring study of mother-child pairs. Environ Int. 75:159–165. https://doi.org/10.1016/j.envint.2014.11.009

Chanput W, Mes JJ, Wichers HJ. 2014. THP-1 cell line: an in vitro cell model for immune modulation approach. Int Immunopharmacol. 23:37–45. https://doi.org/10.1016/j.intimp.2014.08.002

Chen Y, Liu Q, Wang Y, Jiang M, Zhang J, Liu Y, Lu X, Tang H, Liu X. 2024. Triphenyl phosphate interferes with the synthesis of steroid hormones through the PPARgamma/CD36 pathway in human trophoblast JEG-3 cells. Environ Toxicol. 39:3400–3409. https://doi.org/10.1002/tox.24186

Daigneault M, Preston JA, Marriott HM, Whyte MK, Dockrell DH. 2010. The identification of markers of macrophage differentiation in PMA-stimulated THP-1 cells and monocyte-derived macrophages. PLoS One. 5:e8668. https://doi.org/10.1371/journal.pone.0008668

Ding J, Xu Z, Huang W, Feng L, Yang F. 2016. Organophosphate ester flame retardants and plasticizers in human placenta in Eastern China. Sci Total Environ. 554-555:211–217. https://doi.org/10.1016/j.scitotenv.2016.02.171

Doherty BT, Hammel SC, Daniels JL, Stapleton HM, Hoffman K. 2019. Organophosphate esters: are these flame retardants and plasticizers affecting children's health? Curr Environ Health Rep. 6:201–213. https://doi.org/10.1007/s40572-019-00258-0

Dou M, Wang L. 2023. A review on organophosphate esters: physiochemical properties, applications, and toxicities as well as occurrence and human exposure in dust environment. J Environ Manage. 325:116601. https://doi.org/10.1016/j.jenvman.2022.116601

Fan X, Kubwabo C, Rasmussen PE, Wu F. 2014. Simultaneous determination of thirteen organophosphate esters in settled indoor house dust and a comparison between two sampling techniques. Sci Total Environ. 491–492:80–86. https://doi.org/10.1016/j.scitotenv.2013.12.127

Giles BH, Kukolj N, Mann KK, Robaire B. 2024. Phenotypic and functional outcomes in macrophages exposed to an environmentally relevant mixture of organophosphate esters in vitro. Environ Health Perspect. 132:87002. https://doi.org/10.1289/EHP13869

Giles BH, Subramaniam NK, Caruana V, Kukolj N, Robaire B, Mann KK. 2025. A mixture of organophosphate esters sex-specifically impacts monocyte-macrophages in Sprague-Dawley rats. Toxicol Sci. 207:148–160. https://doi.org/10.1093/toxsci/kfaf078

Goicoechea L, Conde de la Rosa L, Torres S, Garcia-Ruiz C, Fernandez-Checa JC. 2023. Mitochondrial cholesterol: metabolism and impact on redox biology and disease. Redox Biol. 61:102643. https://doi.org/10.1016/j.redox.2023.102643

Guan F, Wang R, Yi Z, Luo P, Liu W, Xie Y, Liu Z, Xia Z, Zhang H, Cheng Q. 2025. Tissue macrophages: origin, heterogenity, biological functions, diseases and therapeutic targets. Signal Transduct Target Ther. 10:93. https://doi.org/10.1038/s41392-025-02124-y.

Guo Y, Liang C, Zeng MX, Wei GL, Zeng LX, Liu LY, Zeng EY. 2022a. An overview of organophosphate esters and their metabolites in humans: analytical methods, occurrence, and biomonitoring. Sci Total Environ. 848:157669. https://doi.org/10.1016/j.scitotenv.2022.157669

Guo X, Wu B, Xia W, Gao J, Xie P, Feng L, Sun C, Liang M, Ding X, Zhao D, *et al.* 2022b. Association of organophosphate ester exposure with cardiovascular disease among us adults: cross-sectional findings from the 2011-2018 National Health and Nutrition Examination Survey. Chemosphere. 308:136428.

Hao Z, Zhang Z, Lu D, Ding B, Shu L, Zhang Q, Wang C. 2019. Organophosphorus flame retardants impair intracellular lipid metabolic function in human hepatocellular cells. Chem Res Toxicol. 32:1250–1258. https://doi.org/10.1021/acs.chemrestox.9b00058

He C, English K, Baduel C, Thai P, Jagals P, Ware RS, Li Y, Wang X, Sly PD, Mueller JF. 2018. Concentrations of organophosphate flame retardants and plasticizers in urine from young children in Queensland, Australia and associations with environmental and behavioural factors. Environ Res. 164:262–270. https://doi.org/10.1016/j.envres.2018.02.040

Hoffman K, Butt CM, Webster TF, Preston EV, Hammel SC, Makey C, Lorenzo AM, Cooper EM, Carignan C, Meeker JD, *et al.* 2017. Temporal trends in exposure to organophosphate flame retardants in the United States. Environ Sci Technol Lett. 4:112–118. https://doi.org/10.1021/acs.estlett.6b00475

Hu W, Jia Y, Kang Q, Peng H, Ma H, Zhang S, Hiromori Y, Kimura T, Nakanishi T, Zheng L, *et al.* 2019. Screening of house dust from Chinese homes for chemicals with liver x receptors binding activities and characterization of atherosclerotic activity using an in vitro macrophage cell line and APOE-/- mice. Environ Health Perspect. 127:117003. https://doi.org/10.1289/EHP5039

Huang J, Gao Z, Hu G, Su G. 2022. Non-target screening and risk assessment of organophosphate esters (OPES) in drinking water resource water, surface water, groundwater, and seawater. Environ Int. 168:107443. https://doi.org/10.1016/j.envint.2022.107443

Kubwabo C, Fan X, Katuri GP, Habibagahi A, Rasmussen PE. 2021. Occurrence of aryl and alkyl-aryl phosphates in Canadian house dust. Emerg Contam. 7:149–159. https://doi.org/10.1016/j.emcon.2021.07.002

Lee SJ, Qin H, Benveniste EN. 2008. The IFN-gamma-induced transcriptional program of the CIITA gene is inhibited by statins. Eur J Immunol. 38:2325–2336. https://doi.org/10.1002/eji.200838189

Li Z, Robaire B, Hales BF. 2023a. The organophosphate esters used as flame retardants and plasticizers affect H295R adrenal cell phenotypes and functions. Endocrinology. 164:bqad119. https://doi.org/10.1210/endocr/bqad119

Li M, Wang M, Wen Y, Zhang H, Zhao GN, Gao Q. 2023b. Signaling pathways in macrophages: molecular mechanisms and

therapeutic targets. MedComm (2020). 4:e349. https://doi.org/10.1002/mco2.349

Liu H, Chen YG. 2022. The interplay between TGF-beta signaling and cell metabolism. Front Cell Dev Biol. 10:846723. https://doi.org/10.3389/fcell.2022.846723

Luo K, Zhang R, Aimuzi R, Wang Y, Nian M, Zhang J. 2020. Exposure to organophosphate esters and metabolic syndrome in adults. Environ Int. 143:105941. https://doi.org/10.1016/j.envint.2020.105941

Mazein A, Watterson S, Hsieh WY, Griffiths WJ, Ghazal P. 2013. A comprehensive machine-readable view of the mammalian cholesterol biosynthesis pathway. Biochem Pharmacol. 86:56–66. https://doi.org/10.1016/j.bcp.2013.03.021

McAlister GC, Nusinow DP, Jedrychowski MP, Wuhr M, Huttlin EL, Erickson BK, Rad R, Haas W, Gygi SP. 2014. Multinotch MS3 enables accurate, sensitive, and multiplexed detection of differential expression across cancer cell line proteomes. Anal Chem. 86:7150–7158. https://doi.org/10.1021/ac502040v

Negi CK, Gadara D, Bajard L, Spacil Z, Blaha L. 2025. 2-Ethylhexyl diphenyl phosphate affects steroidogenesis and lipidome profile in human adrenal (H295R) cells. Chem Res Toxicol. 38:733–744. https://doi.org/10.1021/acs.chemrestox.5c00030

Nolfi-Donegan D, Braganza A, Shiva S. 2020. Mitochondrial electron transport chain: oxidative phosphorylation, oxidant production, and methods of measurement. Redox Biol. 37:101674. https://doi.org/10.1016/j.redox.2020.101674

Patisaul HB, Behl M, Birnbaum LS, Blum A, Diamond ML, Rojello Fernandez S, Hogberg HT, Kwiatkowski CF, Page JD, Soehl A, *et al.* 2021. Beyond cholinesterase inhibition: developmental neurotoxicity of organophosphate ester flame retardants and plasticizers. Environ Health Perspect. 129:105001. https://doi.org/10.1289/EHP9285

Pratt JM, Petty J, Riba-Garcia I, Robertson DH, Gaskell SJ, Oliver SG, Beynon RJ. 2002. Dynamics of protein turnover, a missing dimension in proteomics. Mol Cell Proteomics. 1:579–591. https://doi.org/10.1074/mcp.m200046-mcp200

Qiu G, Hill JS. 2007. Atorvastatin decreases lipoprotein lipase and endothelial lipase expression in human THP-1 macrophages. J Lipid Res. 48:2112–2122. https://doi.org/10.1194/jlr.M600510-JLR200

Reines D. 2020. Recent advances in understanding RNA polymerase II structure and function. Fac Rev. 9:11. https://doi.org/10.12703/b/9-11

Remmerie A, Scott CL. 2018. Macrophages and lipid metabolism. Cell Immunol. 330:27–42. https://doi.org/10.1016/j.cellimm.2018.01.020

Rodgers TFM, Truong JW, Jantunen LM, Helm PA, Diamond ML. 2018. Organophosphate ester transport, fate, and emissions in Toronto, Canada, estimated using an updated multimedia urban model. Environ Sci Technol. 52:12465–12474. https://doi.org/10.1021/acs.est.8b02576

Samuel W, Nagineni CN, Kutty RK, Parks WT, Gordon JS, Prouty SM, Hooks JJ, Wiggert B. 2002. Transforming growth factor-beta regulates stearoyl coenzyme a desaturase expression through a SMAD signaling pathway. J Biol Chem. 277:59–66. https://doi.org/10.1074/jbc.M108730200

Shi C, Pamer EG. 2011. Monocyte recruitment during infection and inflammation. Nat Rev Immunol. 11:762–774. https://doi.org/10.1038/nri3070

Sun Y, Gong X, Lin W, Liu Y, Wang Y, Wu M, Kannan K, Ma J. 2018. Metabolites of organophosphate ester flame retardants in urine from Shanghai, China. Environ Res. 164:507–515. https://doi.org/10.1016/j.envres.2018.03.031

Tall AR, Yvan-Charvet L. 2015. Cholesterol, inflammation and innate immunity. Nat Rev Immunol. 15:104–116. https://doi.org/10.1038/nri3793

van der Veen I, de Boer J. 2012. Phosphorus flame retardants: properties, production, environmental occurrence, toxicity and analysis. Chemosphere. 88:1119–1153. https://doi.org/10.1016/j.chemosphere.2012.03.067

Wade MG, Kawata A, Rigden M, Caldwell D, Holloway AC. 2019. Toxicity of flame retardant isopropylated triphenyl phosphate: liver, adrenal, and metabolic effects. Int J Toxicol. 38:279–290. https://doi.org/10.1177/1091581819851502

Wang X, Chen P, Zhao L, Zhu L, Wu F. 2021. Transplacental behaviors of organophosphate tri- and diesters based on paired human maternal and cord whole blood: efficiencies and impact factors. Environ Sci Technol. 55:3091–3100. https://doi.org/10.1021/acs.est.0c06095

Wang S, Link F, Han M, Chaudhary R, Asimakopoulos A, Liebe R, Yao Y, Hammad S, Dropmann A, Krizanac M, *et al.* 2024a. The interplay of TGF-beta1 and cholesterol orchestrating hepatocyte cell fate, EMT, and signals for HSC activation. Cell Mol Gastroenterol Hepatol. 17:567–587. https://doi.org/10.1016/j.jcmgh.2023.12.012

Wang X, Luu T, Beal MA, Barton-Maclaren TS, Robaire B, Hales BF. 2022a. The effects of organophosphate esters used as flame retardants and plasticizers on granulosa, Leydig, and spermatogonial cells analyzed using high-content imaging. Toxicol Sci. 186:269–287. https://doi.org/10.1093/toxsci/kfac012

Wang X, Rowan-Carroll A, Meier MJ, Yauk CL, Wade MG, Robaire B, Hales BF. 2024b. House dust-derived mixtures of organophosphate esters alter the phenotype, function, transcriptome, and lipidome of KGN human ovarian granulosa cells. Toxicol Sci. 200:95–113. https://doi.org/10.1093/toxsci/kfae052

Wang X, Wang L, Li F, Teng Y, Ji C, Wu H. 2022b. Toxicity pathways of lipid metabolic disorders induced by typical replacement flame retardants via data-driven analysis, in silico and in vitro approaches. Chemosphere. 287:132419. https://doi.org/10.1016/j.chemosphere.2021.132419

Werb Z, Cohn ZA. 1971. Cholesterol metabolism in the macrophage. I. The regulation of cholesterol exchange. J Exp Med. 134:1545–1569.

Wu Y, Yao Y, Chen S, Li X, Wang Z, Wang J, Gao H, Chen H, Wang L, Sun H. 2025. Target and nontarget analysis of organophosphorus flame retardants and plasticizers in a river impacted by industrial activity in Eastern China. Environ Sci Technol. 59:798–810. https://doi.org/10.1021/acs.est.4c09875

Yadav H, Quijano C, Kamaraju AK, Gavrilova O, Malek R, Chen W, Zerfas P, Zhigang D, Wright EC, Stuelten C, *et al.* 2011. Protection from obesity and diabetes by blockade of TGF-beta/SMAD3 signaling. Cell Metab. 14:67–79. https://doi.org/10.1016/j.cmet.2011.04.013

Yang R, Bian H, Zhou Z, Yang Y, Wang X, Xu J, Zhong W, Zhu L. 2025. Underlying mechanisms of metabolic dysfunction-associated steatotic liver disease induced by 2-ethylhexyl diphenyl phosphate and its hydroxylated metabolite in zebrafish (*Danio rerio*). J Hazard Mater. 493:138407. https://doi.org/10.1016/j.jhazmat.2025.138407

Yu D, Hales BF, Robaire B. 2024. Organophosphate ester flame retardants and plasticizers affect the phenotype and function of HEPG2 liver cells. Toxicol Sci. 199:261–275. https://doi.org/10.1093/toxsci/kfae034

Yu D, Hales BF, Robaire B. 2025. Effects of an environmentally relevant mixture of organophosphate esters on the phenotype and function of HEPG2 liver cells. Arch Toxicol. 99:5005–5022. https://doi.org/10.1007/s00204-025-04173-2

Zhang D, Liu X, Tu J, Xiao Q, Han L, Fu J, Bian J, Zhang R, Chen J, Shao Y, *et al.* 2024. Mediating role of glucose-lipid metabolism in the

association between the increased risk of coronary heart disease and exposure to organophosphate esters, phthalates, and polycyclic aromatic hydrocarbons. Environ Health (Wash). 2:170–179. https://doi.org/10.1021/envhealth.3c00155

Zhang X, Suhring R, Serodio D, Bonnell M, Sundin N, Diamond ML. 2016. Novel flame retardants: estimating the physical-chemical properties and environmental fate of 94 halogenated and organophosphate PBDE replacements. Chemosphere. 144:2401–2407. https://doi.org/10.1016/j.chemosphere.2015.11.017

Zhu Q, Kanneganti TD. 2017. Cutting edge: distinct regulatory mechanisms control proinflammatory cytokines IL-18 and IL-1β. J Immunol. 198:4210–4215. https://doi.org/10.4049/jimmunol.1700352

Toxicological Sciences, 2026, 209, 1–14
https://doi.org/10.1093/toxsci/kfag048
Research article